BULLETIN DE L'ASSOCIATION MINERALOGIQUE DU CANADA

THE CANADIAN MINERALOGIST

JOURNAL OF THE MINERALOGICAL ASSOCIATION OF CANADA

Volume 36 June 1998 Part 3

The Canadian Mineralogist
Vol. 36, pp. 683-700 (1998)

THE ACCUMULATION OF RARE-EARTH AND HIGH-FIELD-STRENGTH ELEMENTS IN PERALKALINE GRANITIC ROCKS: THE GALIÑEIRO ORTHOGNEISSIC COMPLEX, NORTHWESTERN SPAIN

PILAR MONTERO[1]

Centro de Instrumentación Científica, Universidad de Granada, Campus Fuentenueva, E-18002 Granada, Spain

PETER FLOOR[1]

Leiden University Office, PO Box 9500, 2300 RA Leiden, Netherlands

GUILLERMO CORRETGÉ[1]

Departamento de Geología, Universidad de Oviedo, E-33005 Oviedo, Spain

ABSTRACT

The Galiñeiro complex, in the Iberian Hercynian belt, is composed of pre-Hercynian gneissic peralkaline granitic rocks that host hydrothermal mineralization of rare-earth and high-field-strength elements. The *REE* and *HFSE* are hosted by a large variety of accessory minerals such as bastnäsite, *REE* silicates (*e.g.*, allanite, thalenite – yttrialite), *REE* niobotantalates (aeschynite, fergusonite – formanite, samarskite, pyrochlore – betafite), *REE* phosphates (monazite, xenotime), Th-rich minerals (thorite, P-rich thorite), and zircon. The original magma was derived from a mantle source and most likely had a volatile-rich alkaline basalt composition that evolved by crystal fractionation to give peralkaline silicic differentiates that crystallized at high levels in the crust 460–480 Ma ago. Magmatic fractionation produced residual fluids extremely enriched in fluorine and other ligands, which complexed the rare earths and high-field-strength elements. The decrease in fluorine activity related to falling temperature and the crystallization of F-bearing major minerals produced the breakdown of complexes, releasing the rare earths and the rest of the high-field-strength elements, which then precipitated *HFSE*- and *REE*-rich minerals. The elevated fluorine, CO_2 and sulfide contents of the Galiñeiro system, together with the energy inputs related to different phases of the Hercynian metamorphism, caused episodic remobilization, reflected by the zircon U–Pb concordant ages at 370 and 310 Ma, and the exotic geochemical features (Zr/Hf > 100, elevated levels of Be, Th, and *HREE*) of some samples.

Keywords: Galiñeiro peralkaline complex, accessory minerals, *REE–HFSE* mineralization, metasomatism, fluorine, Spain.

---

[1] *E-mail addresses*: pmontero@goliat.ugr.es, pfloor@bvdu.leidenuniv.nl, corretge@asturias.geol.uniovi.es

SOMMAIRE

Le complexe de Galiñeiro, faisant partie de la chaîne hercynienne dans la péninsule ibérique, contient des roches gneissiques anté-hercyniennes dont la composition rappelle les granites hyperalcalins; ces roches ont été enrichies en terres rares et en éléments à champ électrostatique élevé par voie hydrothermale. Ces éléments traces ont comme hôtes une grande variété de minéraux accessoires, par exemple la bastnäsite, des silicates de terres rares, (*e.g.*, allanite, thalenite – yttrialite), des niobotantalates de terres rares (aeschynite, fergusonite – formanite, samarskite, pyrochlore – bétafite), des phosphates de terres rares (monazite, xénotime), des minéraux de Th (thorite, thorite riche en P), et zircon. Le magma originnel est issue d'une source dans le manteau, et aurait eu une composition de basalte alcalin enrichi en phase volatile; sa composition a évolué par cristallisation fractionnée pour mener à des magmas siliceux hyperalcalins qui ont cristallisé à faible profondeur dans la croûte il y a environ 460–480 Ma. Le fractionnement magmatique a produit des fluides résiduels extrêmement enrichis en fluor et autres ligands, qui ont complexé les terres rares et les éléments à champ électrostatique élevé. Une diminution de l'activité du fluor liée à une diminution de la température et à la cristallisation de minéraux majeurs contenant du fluor a causé une déstabilisation des complexes hydrothermaux, et une libération des cations complexés, qui ont par la suite précipité sous forme de minéraux accessoires. Les teneurs élevées en fluor, CO_2 et sulfures des roches du cortège de Galiñeiro, ainsi que l'ajout d'énergie liée aux diverses phases de métamorphisme hercynien, ont causé une remobilisation épisodique, comme en témoignent les interceptes dans le système U–Pb du zircon, dont les âges concordants seraient de 370 et 310 Ma, et les caractéristiques géochimiques exotiques (Zr/Hf > 100, teneurs élevées de Be, Th, et terres rares lourdes) dans certains échantillons.

(Traduit par la Rédaction)

Mots-clés: complexe hyperalcalin de Galiñeiro, minéraux accessoires, terres rares, éléments à potentiel ionique élevé, enrichissement hydrothermal, métasomatose, fluor, Espagne.

INTRODUCTION

The Galiñeiro complex is a small intrusive body that crops out in the allochthonous Malpica – Tuy Unit, Iberian Hercynian belt. It is mainly composed of pre-Hercynian gneissic peralkaline granitic rocks that host hydrothermal enrichment of the rare-earth elements (REE) and high-field-strength elements (HFSE) (Floor 1966, Rambaud *et al.* 1992, Montero 1993, Martín-Izard *et al.* 1995). Other peralkaline felsic rocks of similar age and field relationships are widely distributed in Iberia (Ribeiro & Floor 1988), although none have the enrichment in rare-earth and high-field-strength elements seen in the Galiñeiro complex. In this respect, the Galiñeiro complex may be compared to the mineralized peralkaline granites of Ghurayyah and Umm al Birak in the Arabian Shield (Jackson *et al.* 1985), or to granites from the central part of the Kola Peninsula (Belkov 1979, Belkov *et al.* 1988, Belolipetskii & Voloshin 1996). The rare-earth and high-field-strength elements of the Galiñeiro rocks are contained in a large variety of accessory minerals, such as bastnäsite, rare-earth silicates, rare-earth niobotantalates, Th-rich minerals, and zircon. Since the unmineralized peralkaline orthogneisses contain the same assemblage of accessory phases as the hydrothermally enriched rocks, though these obviously are less abundant, the Galiñeiro complex is a good example with which to study the accumulation of the rare-earth and high-field-strength elements in peralkaline systems and to determine the origin of the ore-forming fluids.

In this paper, we summarize current knowledge concerning the Galiñeiro complex, acquired as a result of the field, mineralogical, and petrographic work of Floor (1966) and the later geochemical and isotopic work of Montero (1993). We have two objectives. On one hand, we intend to decipher the complex history of Galiñeiro rocks and their evolution in the framework of the Iberian belt. On the other, we wish to provide insight into the mechanisms of accumulation of the rare-earth and high-field-strength elements up to economic levels in a peralkaline felsic system.

ANALYTICAL METHODS

Samples

About one hundred and fifty samples (minimum 5 kg per sample) from surface and drill holes were collected for this study. Thin sections were prepared for optical and scanning electron microscopy, electron microprobe, and, in certain cases, for laser-ablation microprobe – inductively coupled plasma – mass spectrometry (LAM–ICP–MS). Powders were obtained for analysis by reducing the rocks in a crusher with hardened jaws to a grain size of less than 5 mm and then grinding them in a tungsten carbide jar to a grain size of less than 25 μm. This procedure produced no detectable contamination of rare-earth or high-field-strength elements.

Whole-rock analyses

Major-element analyses were carried out by inductively coupled plasma – optical emission spectrometry (ICP–OES) after digesting 0.2 g of sample powder with a mixture of HNO_3 and HF under pressure in a teflon-lined vessel at a controlled temperature.

Instrument measurements were carried out with a Perkin Elmer Plasma II spectrometer using the Myers–Tracy signal-compensation system. Coefficients of variation were about 0.25, 0.75 and 2.5% for analyte concentrations of 10, 1 and 0.1 wt.%, respectively. Concentrations of the trace elements, including the rare earths, were determined by inductively coupled plasma – mass spectrometry (ICP–MS) after HNO_3 + HF digestion of 0.1 g of sample powder in a teflon-lined vessel at high temperature and pressure, evaporation to dryness, and dissolution in 100 mL of 4 vol.% HNO_3. Instrument measurements were performed with a Perkin Elmer Sciex ELAN 5000 spectrometer, using Re and Rh as internal standards. Coefficients of variation were about 2 and 5% for analyte concentrations of 50 and 5 ppm, respectively. The concentration of fluorine was determined by X-ray fluorescence (XRF) with a precision of 5%.

Mineral analyses

Concentrations of the major elements in the rock-forming minerals were determined with a Cameca CAMEBAX SX–50 electron microprobe, using an accelerating voltage of 15 kV, a beam current of 15 nA, and a counting time of 10 s (peak) and 5 s (background). The concentrations of the rare-earth elements, Y, Th, and U in accessory minerals were determined with an ARL electron microprobe operated with PROBE software. Accelerating voltage was 20 kV, beam current was 20 nA, and counting times were 30 s (peak) and 10 s (background). As standards, we used the four synthetic glasses of Drake & Weill (1972), and the following synthetic phases: Albite Amelia Chgo/18, Mn-Hortonolite Chgo/35, Monazite SPI/32, and Zirconia SPI/47. Interelement interferences were suppressed with peak-overlap corrections (Roeder 1985). Detection limits were better than 0.10–0.05% depending on the element determined and the mineral analyzed. Coefficients of variation were close to 4 and 10% for analyte concentrations of 1 and 0.25 wt.%, respectively. Analyses of zircon were performed by LAM–ICP–MS in the Perkin Elmer ICP–MS Applications Laboratory at Überlingen, Germany, with a prototype UV laser-ablation system coupled to a high-sensitivity PE Sciex ELAN–6000 ICP–MS spectrometer, following the method described by Bea *et al.* (1996).

Isotopic analyses

Samples for Rb/Sr and Sm/Nd dating were prepared using whole-rock powders following conventional methods of sample digestion and chromatographic separation. Isotopic analyses were carried out with a Finnigan MAT 262 multi-collector mass spectrometer. Standard errors at 2σ level were 0.5% for $^{87}Rb/^{86}Sr$ and 0.01–0.02% for $^{87}Sr/^{86}Sr$. Standard errors (2σ) for $^{143}Nd/^{144}Nd$ were 0.003%, and for $^{147}Sm/^{144}Nd$, 0.3%. U/Pb analyses were performed on zircon concentrates, and all isotopic ratios were measured on a Cameca TSN–206 mass spectrometer; standard errors at the 2σ level were 0.1% for $^{207}Pb/^{206}Pb$ and $^{208}Pb/^{206}Pb$, and 1–3% for $^{206}Pb/^{204}Pb$. $^{207}Pb/^{206}Pb$ analyses on single crystals of zircon were performed on a Finnigan MAT 262 by direct evaporation.

GEOLOGICAL SETTING AND PETROGRAPHY

The Galiñeiro orthogneissic complex has a roughly circular exposure of about 10 km². It intrudes the southern part of the Malpica – Tuy Unit (Ortega & Gil Ibarguchi 1983), an allochthonous terrane mainly consisting of Upper Proterozoic metasedimentary rocks and Ordovician orthogneisses overthrust on the Western Galicia Domain, in the Central Iberian Zone (Arenas *et al.* 1988, Farias *et al.* 1987) (Fig. 1).

The Galiñeiro complex is mainly composed of two rock types, aegirine – riebeckite gneisses and amphibole – biotite gneisses. Intimately associated with the above are small patches and veins of hydrothermally affected rocks having biotite as the only mafic mineral and containing such an elevated abundances of Th-rich accessory phases that they were called "radioactive" gneisses by field geologists (Arribas 1963, Floor 1966).

Aegirine – riebeckite gneisses represent more than 95% of the outcrops in the complex. Their major mineral assemblage is composed of quartz, nonperthitic microcline (Or ≈ 97%), sodic plagioclase (Ab ≈ 98%), riebeckite – arfvedsonite, Al-poor aegirine, and subordinate annite (Fe/[Fe + Mg] ≈ 0.9). Accessory minerals, described in detail in the next section, are extraordinarily abundant and include a plethora of *REE*- or *HFSE*-rich species together with fluorite, titanite, magnetite, ilmenite, and sulfides. Aegirine – riebeckite gneisses are classified into three facies, according to their major mineralogy and fabric (Floor 1966): (1) the Galiñeiro facies, the most abundant, (2) the Zorro facies, characterized by the presence of larger and more abundant porphyroblasts of microcline than the Galiñeiro facies, and (3) the Magnetite facies, characterized by the presence of conspicuous crystals of magnetite.

Amphibole – biotite gneisses represent less than 5% of the exposed surface. Their composition varies from dioritic to granitic, but the most common rock-type is a leucotonalite with an assemblage of major minerals composed of quartz, oligoclase (Ab ≈ 87%), nonperthitic K-feldspar (Or ≈ 96%), biotite (0.63 < Fe/[Fe + Mg] < 0.69), and hastingsitic amphibole. Accessory minerals are zircon, titanite, apatite, fluorite, ore minerals, and garnet. In contrast with aegirine – riebeckite gneisses, ampibole – biotite gneisses contain only minor *REE*-rich minerals.

"Radioactive" gneisses (hereafter called R-gneisses) have the highest accumulations of rare metals and are

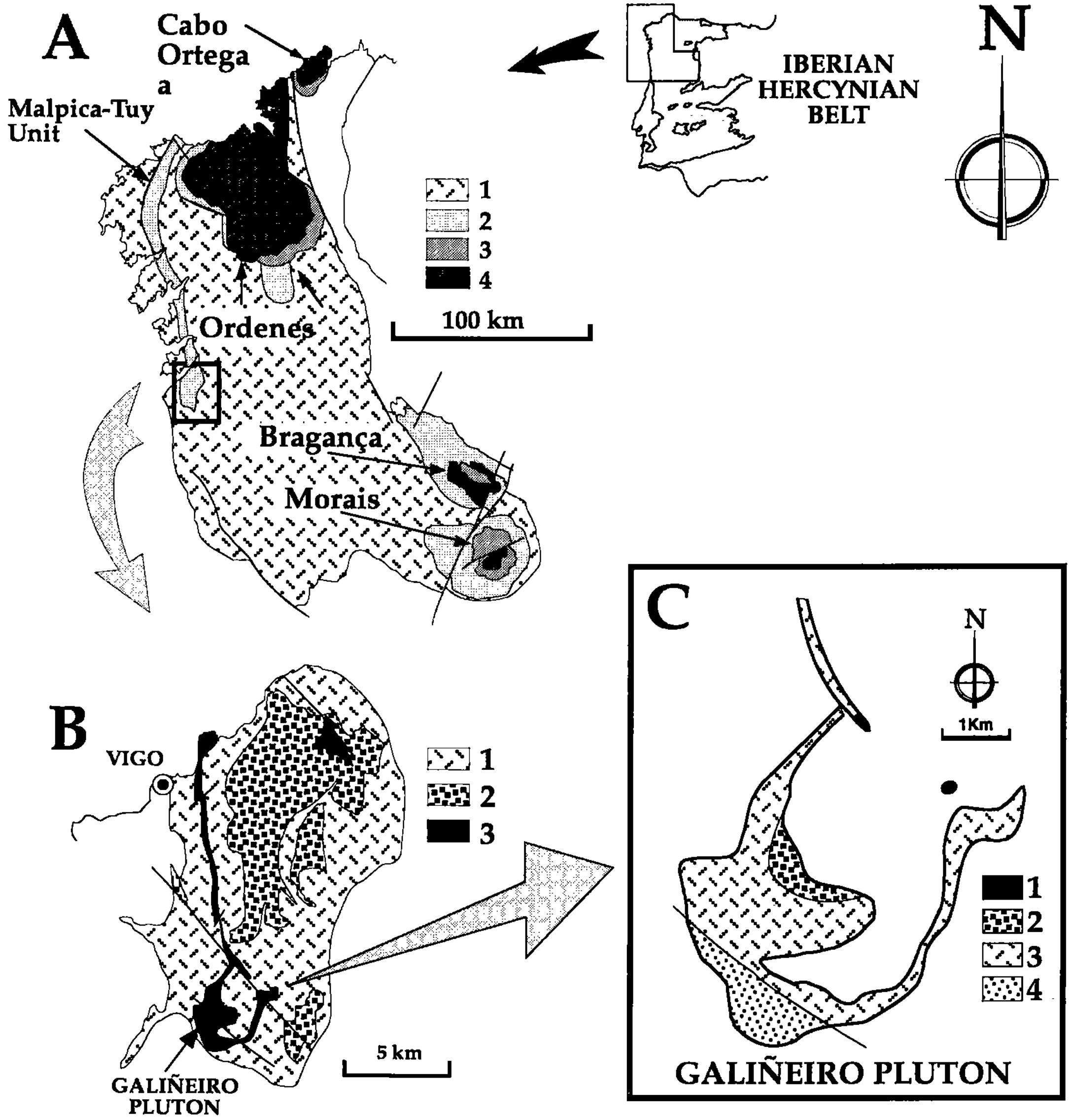

FIG. 1. A. Tectonostratigraphic map of the Western Iberian Hercynian Belt. 1. Central Iberian and Galicia Trás-os-Montes autochthon-parautochthon. 2. Lower allochthon with peralkaline rocks. 3. Ophiolitic complex. 4. Upper allochthon with HP–HT granulites and eclogites. B. Simplified map of the southern Malpica – Tuy Unit. 1 Paragneisses and schists. 2 Biotite orthogneisses. 3 Peralkaline acid rocks. A and B after Pin *et al.* (1992). C. Schematic distribution of aegirine – riebeckite gneisses and R-gneisses from the Galiñeiro complex, simplified from Floor (1966); 1 R-gneisses, 2 Magnetite facies, 3 Galiñeiro facies, 4 Zorro facies.

by far the least abundant rock-type in the Galiñeiro complex, comprising less than 1% of the outcrop area. As they have been prospected, most samples studied here were taken from drill-cores. Two subtypes can be distinguished on the basis of mineralogy (Montero 1993): (1) R–1 gneisses, composed of albite (Ab ≈ 98%), quartz, annite (Fe/[Fe + Mg] ≈ 0.9), gruneritic amphibole, with no K-feldspar and an elevated abundance of *REE-* and *HFSE*-rich accessories (up to 5 vol.%); (2) R–2 gneisses, composed of quartz, albite–oligoclase, biotite (0.4 < Fe/[Fe + Mg] ≈ < 0.95), K-feldspar (Or ≈ 97%), and occasional minor riebeckite and aegirine; the modal proportion of accessories is rarely over 1%.

The Galiñeiro complex was deformed and metamorphosed during the Hercynian Orogeny, which led to total recrystallization of the original assemblage in the lower amphibolite facies and caused the foliated to lineated fabric characteristic of these rocks. Geothermobarometric studies (Montero 1993) indicate that they equilibrated at 400–550°C and 0.5–0.6 GPa, although regional equilibrium persisted until much lower pressures, as indicated by the presence of stable cordierite, andalusite and cummingtonite in the host rocks (Floor 1966).

The paragneisses surrounding the Galiñeiro complex show evidence of metasomatic alteration, especially intense near the contact with the main peralkaline body (Floor 1966), which mainly involved of the input of sodium and generated new crystals of albite.

The Assemblage of Accessory Minerals

In the Galiñeiro rocks, the entire budget of rare-earth and high-field-strength elements is hosted by accessory minerals. Optical, scanning electron microscopy (SEM) and electron-microprobe studies allowed the identification of rare-earth carbonates (bastnäsite, parisite), rare-earth niobotantalates (fergusonite – formanite, samarskite, aeschynite and pyrochlore – betafite), silicates of the rare-earths and Y (allanite, thalenite – yttrialite group phases), rare-earth phosphates (monazite, xenotime), Th orthosilicates (thorite, huttonite, P-rich thorite), titanite, zircon and occasional rare-earth fluorides (fluocerite). Other abundant accessories are fluorite, astrophyllite, chlorite, sulfides, magnetite, and ilmenite. *REE*- and *HFSE*-rich minerals may appear either as isolated crystals (generally included in major minerals, such as feldspar and riebeckite) or, more commonly, forming complex polycrystalline aggregates with a maximum dimension ranging from 0.1 to 1 mm. Aggregates are very irregular in shape and composition; several phases may coexist, although one or two are usually dominant. Zircon- and bastnäsite-based aggregates are the most abundant, but aggregates formed essentially of niobotantalates, thorite, rare-earth phosphates and locally rare-earth-Y silicates also are very common. In many cases, no one mineral predominates. Secondary bastnäsite, parisite, monazite, and thorite also appear filling small fractures and cavities.

Zircon

Zircon, the most common accessory, can account for 10 vol.% of some R–1 samples. It normally forms aggregates of brown turbid rounded crystals, usually less than 50 μm in diameter, commonly associated with other accessory phases. Less commonly, well-developed crystals with a maximum size close to 300 μm are found. According to Pupin & Turco (1972), these crystals belong to *A* and, rarely, *G* and *P* morphological types, corresponding to zircon crystallized in a peralkaline environment at low temperatures (<650°C). Remarkably, crystals with a morphology indicative of higher temperatures are seldom found.

LAM–ICP–MS analyses reveal that zircon crystals usually have low concentrations of Th, U, Y and the rare-earth elements (Table 1). Chondrite-normalized

Table 1. REE, Th and U concentrations in zircon, bastnäsite and parisite from the Galiñeiro complex

	Zircon		*Bastnäsite*				*Parisite*	
	1	2	7	8	3	2	1	2
(ppm)								
Y	139	0.97	1343	2686	948	790	6557	1106
U	259	0.76	n.d.	n.d.	n.d.	n.d.	n.d.	n.d.
Th	28.1	-	-	-	-	-	21500	9800
La	1.65	1.63	207500	180900	192800	212600	116400	109900
Ce	5.37	3.16	254400	247500	262400	264000	279900	281200
Pr	0.50	0.47	25400	27100	27000	25100	40400	38800
Nd	3.34	1.31	78900	96900	87800	79600	78800	78800
Sm	2.45	0.45	9800	20200	11200	9486	850	1440
Eu	1.15	0.05	950	1640	1550	1120	-	-
Gd	8.90	0.53	3730	8940	5380	3470	-	-
Tb	4.41	0.13	n.d.	n.d.	n.d.	n.d.	n.d.	n.d.
Dy	47.3	0.74	-	-	-	-	78	-
Ho	19.0	0.23	n.d.	n.d.	n.d.	n.d.	n.d.	n.d.
Er	82.5	0.96	-	-	-	-	-	-
Tm	20.4	0.16	n.d.	n.d.	n.d.	n.d.	n.d.	n.d.
Yb	187	1.20	-	-	-	-	518	-
Lu	27.1	0.26	-	-	-	-	-	-

Zircon analyzed by LAM-ICP MS (ppm). Bastnäsite and Parisite analyzed by electron microprobe (ppm). n.d. not determined. - below detection limit.

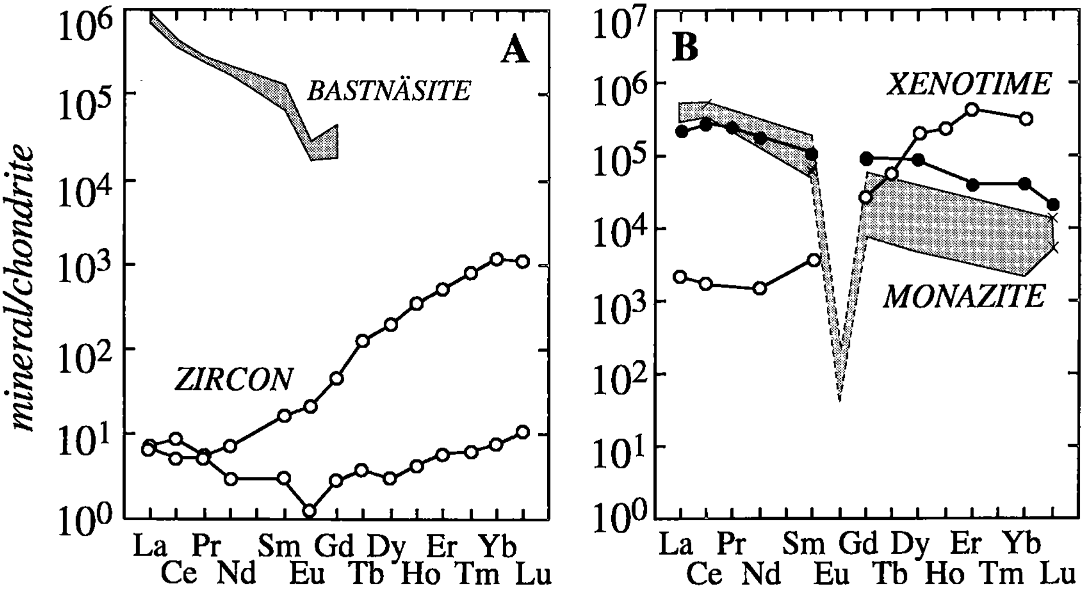

FIG. 2. A. The grey area comprises several chondrite-normalized *REE*-patterns of bastnäsite. Elements not shown are below detection limit. At the bottom of the diagram are two selected patterns of *REE*-rich zircon crystals. B. Grey area defined by several *REE*-patterns of primary monazite. Superimposed pattern (black dots) corresponds to a secondary monazite, and white dots, to xenotime.

REE patterns (Fig. 2A) have a modest positive slope, with $La_N/Lu_N \approx 0.6–0.7$, and a negative Eu anomaly. Only in those anomalous samples enormously enriched in the heavy rare-earths (see below) does zircon have elevated concentrations of these elements, with $La_N/Lu_N \approx 0.006$, and no Eu anomaly.

REE carbonates: bastnäsite and parisite

Bastnäsite is the most important host of the light rare-earth elements in the Galiñeiro rocks. It can be found (1) as isolated crystals, locally included in feldspars, (2) forming aggregates with other accessory phases, and (3) filling small veinlets and cavities. Isolated crystals are xenomorphic and usually smaller than 200–300 μm. Their composition corresponds to bastnäsite-(Ce) (Table 1), with a very low concentration of Y and no detectable Th. Chondrite-normalized *REE* patterns (Fig. 2A) are characterized by a smooth negative profile from La to Sm, a small negative Eu anomaly, and a steep drop in the heavy rare-earth elements, whose concentrations are below the minimum limit of detection for the microprobe.

Parisite is not abundant. It occurs as irregular small crystals or cryptocrystalline aggregates invariably in association with other *REE*-rich minerals, which may probably represent products of its alteration. Its composition corresponds to parisite-(Ce), close to the theoretical value ($\Sigma REE_2O_3 \approx 60.9$ wt.%: Mariano 1989), with Ce > La and very low levels of the heavy rare-earth elements (Table 1). It also has variable but somewhat elevated levels of Th (0.9–2 wt.%) and Y (0.1–0.6 wt.%), significantly higher than those of bastnäsite. The concentration of Ca is close to 9.3 wt.%.

REE phosphates: monazite and xenotime

Monazite follows bastnäsite in importance as a reservoir of the light rare-earth elements. As in the case of bastnäsite, three textural varieties of monazite are recognized: (1) isolated crystals, in some cases included in major minerals, (2) small crystals forming aggregates with other *REE*-rich accessory phases, and (3) irregular crystals filling cracks and veins. In all cases, crystals are xenomorphic and rarely larger than 0.4 mm. The chemical composition of the first two varieties (Table 2) is identical, being characterized by elevated Th and low concentrations of the heavy rare-earth elements and Y, which is compatible with a primary origin (Förster 1993, Förster & Rhede 1995, Bea 1996). In contrast, secondary monazite filling cracks or small cavities invariably has low concentrations of Th but elevated contents of the Ca, Y and heavy rare-earth elements, and flatter chondrite-normalized *REE* patterns, with the same deep negative Eu anomaly (Fig. 2B).

Xenotime is one of the most important reservoirs of the heavy rare-earth elements (*HREE*) in the Galiñeiro complex. It usually forms aggregates with other *REE*-minerals. The crystals are xenomorphic, small (maximum 300 μm) and reddish to pale yellow. Its composition corresponds to xenotime-(Y); $\sum REE_2O_3$ varies from 19.7 to 21.2 wt.%, with Dy and Er as the most abundant rare earths (Table 2). Xenotime crystals commonly are zoned, with a *HREE*-rich rim and a Y-rich core. Chondrite-normalized *REE* patterns have a strong positive slope with a large negative Eu anomaly (Fig. 2B).

Silicates: allanite, titanite, thorite and Y–Yb silicates

Allanite is quite abundant, so that it contains a significant fraction of the light rare-earth elements budget. It usually occurs in aggregates and rarely as individual grains. Crystals are xenomorphic or subidiomorphic, usually smaller than 300–400 μm, and dark brown to yellow. Its composition is very constant (Table 3), similar to that described in other peralkaline granites (Belkov *et al.* 1988), and it shows significantly higher levels of Y, *REE*, and Fe, but lower concentration of Al, Mg and Ca, than allanite from peraluminous and subaluminous granites (Bea 1996). Regarding chondrite-normalized *REE* patterns (Fig. 3A), it is worth mentioning that allanite from Galiñeiro, and other peralkaline rocks, usually shows a much smaller negative Eu anomaly, which probably reflects a higher Eu^{3+}/Eu^{2+} due to more oxidizing conditions, than allanite from peraluminous and subaluminous granites.

Titanite is not abundant, and commonly forms part of the aggregates. It is typically dark brown and less than 100–150 μm across. Chondrite-normalized *REE* patterns show a negative slope in the light rare earths, no Eu anomaly, and a slightly positive slope from middle to heavy rare-earth elements.

Th-orthosilicate minerals, probably thorite according to the rhombic morphology of the scarce well-formed crystals, are widespread in the Galiñeiro suite, accounting for the high radioactivity of these rocks. Similar to bastnäsite and monazite, thorite appears either as individual grains included in major minerals, forming aggregates with other *REE* minerals, or filling small cracks and veins. Crystals are usually xenomorphic, brown to deep red, and range from a few μm up to 1.5–2 mm. Its composition is highly variable,

TABLE 2. REPRESENTATIVE COMPOSITION OF MONAZITE (PRIMARY AND SECONDARY) AND XENOTIME FROM THE GALIÑEIRO COMPLEX

	Primary monazite					*Secondary*		*Xenotime*		
	1	2	3	5	6	7	8	2	3	7
(wt%)										
SiO_2	0.57	0.02	0.09	1.75	1.61	-	0.92	n.d.	n.d.	n.d.
ZrO_2	-	0.24	0.13	0.17	0.03	-	0.35	n.d.	n.d.	n.d.
Al_2O_3	0.16	-	-	-	-	-	0.62	n.d.	n.d.	n.d.
FeO	0.48	-	-	0.03	-	-	0.15	n.d.	n.d.	n.d.
MgO	-	-	-	-	-	-	-	n.d.	n.d.	n.d.
CaO	0.09	0.04	0.04	0.05	0.04	1.90	1.75	n.d.	n.d.	n.d.
Na_2O	-	-	-	-	-	-	0.11	n.d.	n.d.	n.d.
P_2O_5	21.25	28.03	28.89	25.23	25.71	26.04	25.64	35.30	34.85	33.89
Y_2O_3	0.63	1.04	1.08	0.37	0.42	7.98	7.67	42.96	45.12	43.39
ThO_2	15.56	2.06	0.90	10.04	12.47	-	-	0.03	-	0.02
UO_2	0.49	-	-	-	-	0.32	0.48	n.d.	n.d.	n.d.
La_2O_3	7.80	10.25	11.60	12.73	12.49	6.85	6.36	0.12	0.07	0.06
Ce_2O_3	27.29	32.96	35.91	32.43	30.23	21.50	20.92	0.10	0.08	0.12
Pr_2O_3	3.29	4.16	4.40	4.35	4.22	2.49	2.73	-	0.03	-
Nd_2O_3	17.54	15.14	14.16	10.85	10.98	10.12	9.58	0.01	0.10	0.08
Sm_2O_3	3.21	1.84	1.16	0.79	1.00	2.01	1.87	0.01	0.23	0.06
Eu_2O_3	-	-	-	-	-	-	-	-	-	-
Ga_2O_3	1.23	1.32	0.33	0.17	0.48	2.13	2.11	0.70	1.43	0.62
Tb_2O_3	n.d.	n.d.	n.d.	n.d.	n.d.	n.d.	n.d.	0.26	0.50	0.25
Dy_2O_3	0.16	0.12	-	-	-	2.19	2.42	5.63	7.00	5.41
Ho_2O_3	n.d.	n.d.	n.d.	n.d.	n.d.	n.d.	n.d.	1.59	1.60	1.61
Er_2O_3	-	-	-	-	-	0.83	0.77	7.55	5.70	7.54
Yb_2O_3	-	0.06	-	0.04	-	0.76	0.72	5.32	3.00	5.47
Lu_2O_3	-	-	0.02	-	-	0.02	0.20	n.d.	n.d.	n.d.
Total	99.75	97.28	98.71	99.00	99.68	85.14	85.37	99.58	99.71	98.52

Analyses by electron microprobe (%). n.d. not determined. - below detection limit.

TABLE 3. COMPOSITION OF ALLANITE AND THORITE FROM THE GALIÑEIRO COMPLEX

	Allanite				*Thorite*					
	1	2	3	5	1	2	3	4	6	7
(wt%)										
SiO_2	31.03	31.06	31.29	31.63	17.56	18.83	15.63	23.64	9.95	12.60
Al2O3	11.25	11.17	10.75	10.26	0.47	0.37	0.21	0.16	0.19	0.01
FeO	18.68	17.98	18.61	18.23	7.53	1.24	13.42	1.80	0.20	1.70
MgO	0.10	0.10	0.08	0.11	0.03	-	0.03	0.01	0.23	-
MnO	1.48	1.59	1.60	1.45	n.d.	n.d.	n.d.	n.d.	n.d.	n.d.
TiO_2	2.62	2.75	2.48	2.75	n.d.	n.d.	n.d.	n.d.	n.d.	n.d.
CaO	9.27	8.81	9.10	8.77	0.56	0.36	0.16	0.49	3.20	4.51
Na_2O	n.d.	n.d.	n.d.	n.d.	0.15	0.01	0.07	0.02	0.07	0.04
P_2O_5	n.d.	n.d.	n.d.	n.d.	0.55	0.71	0.18	0.58	6.62	10.07
Y_2O_3	0.57	0.55	0.64	0.30	3.14	2.91	3.01	1.43	3.01	3.57
ThO_2	n.d.	n.d.	n.d.	n.d.	55.56	60.82	54.22	57.77	68.21	38.78
UO_2	n.d.	n.d.	n.d.	n.d.	7.37	9.16	9.14	7.85	4.66	1.11
La_2O_3	5.73	4.93	5.36	6.33	-	0.02	-	0.27	0.04	3.99
Ce_2O_3	11.25	11.77	11.26	12.61	0.01	0.09	0.02	0.98	0.15	12.70
Pr_2O_3	1.02	1.30	1.23	1.21	0.01	0.03	-	0.08	0.03	1.65
Nd_2O_3	4.00	5.08	4.06	4.13	0.07	0.27	-	0.27	0.27	4.82
Sm_2O_3	0.74	0.80	0.73	0.55	0.11	0.16	0.18	0.09	0.27	0.90
Eu_2O_3	0.10	0.07	0.07	0.06	0.01	-	-	-	-	0.01
Ga_2O_3	0.39	0.36	0.29	0.27	0.10	0.12	0.07	0.06	0.43	0.93
Tb_2O_3	n.d.	n.d.	n.d.	n.d.	n.d.	n.d.	n.d.	n.d.	n.d.	n.d.
Dy_2O_3	0.22	0.13	0.26	0.13	0.49	0.56	0.43	0.33	1.14	0.96
Er_2O3	n.d.	n.d.	n.d.	n.d.	1.00	0.56	0.45	0.33	0.60	0.45
Yb_2O_3	n.d.	n.d.	n.d.	n.d.	4.63	2.80	2.21	2.56	0.66	0.40
Lu_2O_3	n.d.	n.d.	n.d.	n.d.	0.61	0.37	0.30	0.47	0.06	0.07
Total	98.45	98.45	97.81	98.79	99.96	99.39	99.73	99.19	99.99	99.27

Analyses by electron microprobe (%). n.d. not determined. - below detection limit.

with ThO_2 in the range 55–68 wt.%, FeO_{total} in the range 0–13 wt.%, $Y_2O_3 + \Sigma REE_2O_3$ in the range 6–10 wt.%, and $UO_2 \approx 7$ wt.% (Table 3). Chondrite-normalized *REE* patterns typically have a strong positive slope and a moderate negative Eu anomaly. Some crystals show flatter patterns, with Eu below the detection limit (*e.g.*, anal. 4 and 6, Table 3). Exceptionally, P-rich crystals ($P_2O_5 \approx 10$ wt.%, $ThO_2 < 40$ wt.%, $UO_2 \approx 1$ wt.%) also have been found. Their elevated Y_2O_3 and REE_2O_3 contents and enrichment in light rare-earth elements (Fig. 3B), suggest that they could be isomorphic mixtures with cheralite – monazite.

Y–Yb silicates form polycrystalline aggregates with *REE* niobates, thorite and zircon. Crystals are invariably xenomorphic, dark colored, and less than 100 μm in diameter. Their composition varies between Y-rich and Yb-rich end-members (Table 4). Y-rich varieties have $Y_2O_3 > 20$ wt.%, $SiO_2 > 25$ wt.%, $Yb_2O_3 \approx 1$ wt.% (thalenite – yttrialite?), highly variable amounts of Fe and occasionally elevated Ca (kainosite ?). Yb-rich varieties have $Yb_2O_3 > 35$ wt.%, $SiO_2 \approx 35$ wt.%, $Y_2O_3 \approx$ 13 wt.%, variable concentrations of Fe (hingganite?) and are highly enriched in the heavy rare-earths ($\Sigma HREE_2O_3 > 50$ wt.%). The concentration of Th and U is very low in both cases. Chondrite-normalized *REE* patterns of the Y-rich variety are flat and have a strong negative Eu anomaly. Chondrite-normalized *REE* patterns of the Yb-rich variety, however, have a positive slope with no Eu anomaly (Fig. 4A).

Nb–Ta–REE minerals

These minerals are abundant in R-gneisses, and are also common in aegirine – riebeckite gneisses. They usually appear in aggregates together with other *REE*-accessory minerals. The crystals are xenomorphic, dark-colored, and less than 100–150 μm in size. We identified four extreme compositional types (Table 4, Fig. 4B): (1) *HREE*-rich, with Yb as the dominant *REE*, about 10 wt.% ThO_2 and Y_2O_3, low light rare-earth elements and a strong negative Eu-anomaly (samarskite?); (2) *LREE*-rich, with Ce as the dominant rare-earth element, a deep negative Eu anomaly and variable Th and Y (aeschynite?); (3) Y-rich, moderately enriched in heavy rare-earth elements, with Dy as the dominant rare-earth element and variable Th (fergusonite – formanite?), and (4) U-rich niobates, with low levels of the rare-earth elements and variable but significant levels of Th and Fe (pyrochlore – betafite).

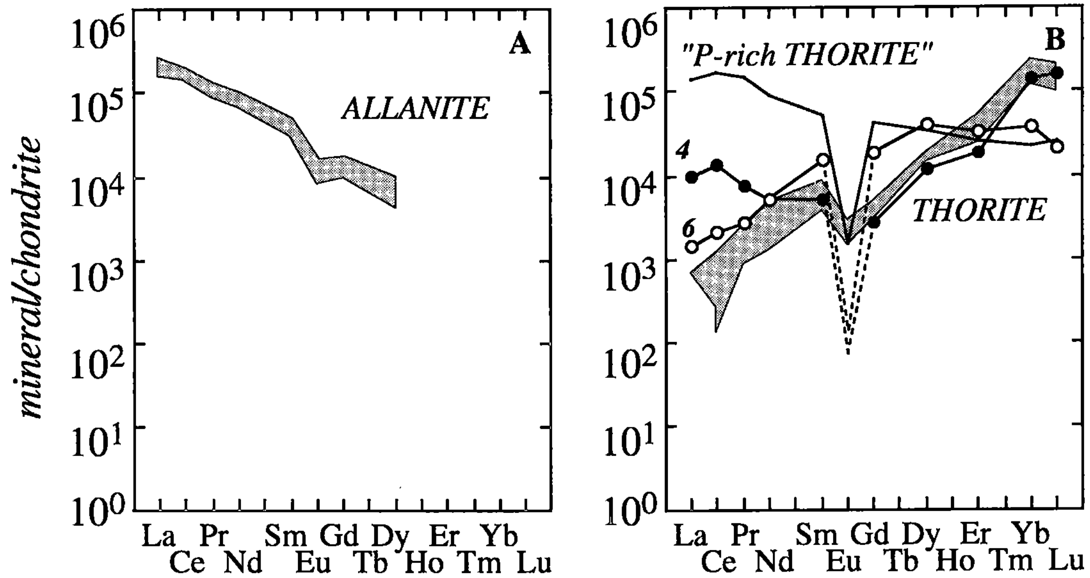

FIG. 3. A. Chondrite-normalized *REE* patterns of allanite and thorite. Grey area defined by several chondrite-normalized patterns of allanite. B. *REE*-patterns of "normal" thorite (grey area). Patterns 4 and 6 pertain to anomalous samples of thorite, and the other pattern corresponds to P-rich thorite.

TABLE 4. REPRESENTATIVE COMPOSITIONS OF REE-SILICATES AND REE-NIOBATES FROM THE GALIÑEIRO COMPLEX

	Y-Yb-silicates				*REE-niobates*					
	2	3	5	6	1	2	3	4	5	6
(wt%)										
SiO_2	35.00	29.45	27.00	32.91	3.14	2.04	8.70	0.17	0.18	1.89
Al_2O_3	-	-	0.21	-	-	0.42	6.86	-	-	0.05
FeO	1.84	0.55	9.99	-	0.44	0.47	1.67	0.51	0.10	4.69
MgO	-	-	-	-	-	-	1.67	-	-	-
CaO	0.08	11.57	0.74	0.27	0.19	1.02	1.95	0.16	0.21	2.95
Na_2O	0.06	0.07	-	0.08	0.11	-	0.02	-	0.02	0.03
P_2O_5	-	0.28	0.02	-	-	0.01	0.07	0.03	0.06	0.02
Y_2O_3	13.45	38.25	21.32	13.21	8.89	4.88	2.71	31.80	29.23	9.08
ThO_2	-	-	-	-	11.54	13.80	1.68	0.48	0.58	2.10
UO_2	-	-	-	-	1.02	-	-	3.85	3.42	29.40
La_2O_3	0.01	0.29	0.81	-	-	10.56	9.94	-	0.03	0.07
Ce_2O_3	0.09	1.31	5.63	0.01	-	22.21	22.36	0.11	0.07	1.02
Pr_2O_3	-	0.18	0.72	-	-	3.34	3.26	0.01	0.02	0.14
Nd_2O_3	0.05	1.47	7.51	-	0.07	7.73	6.63	0.74	0.50	1.03
Sm_2O_3	0.09	1.05	2.68	0.09	0.18	1.06	0.22	1.28	0.86	0.58
Eu_2O_3	-	-	-	0.08	-	-	-	-	-	-
Ga_2O_3	-	2.04	2.98	-	0.12	0.99	0.42	2.41	1.72	0.71
Dy_2O_3	1.01	4.19	2.74	0.76	1.47	0.94	0.14	4.74	6.26	0.91
Er_2O_3	5.99	2.46	1.77	5.40	4.14	0.08	-	2.86	3.76	0.54
Yb_2O_3	35.06	0.72	1.16	40.46	25.58	0.12	-	1.29	1.34	0.28
Lu_2O_3	7.91	0.20	0.17	6.57	3.94	-	-	0.42	0.54	0.07
Total	100.64	94.08	85.45	99.84	60.83	69.67	68.30	50.86	48.90	55.56

Analyses by electron microprobe (%). - below detection limit.
Nb, Ti, and Ta have been identified by means of XR-spectra in every case, but not quantitatively determined. Silicates 2 and 6 are Yb-rich, 3 and 5 are Y-rich. Niobate 1 is HREE-rich, 2 and 3 are LREE-rich, 4 and 5 are Y-rich and niobate 6 is U-rich.

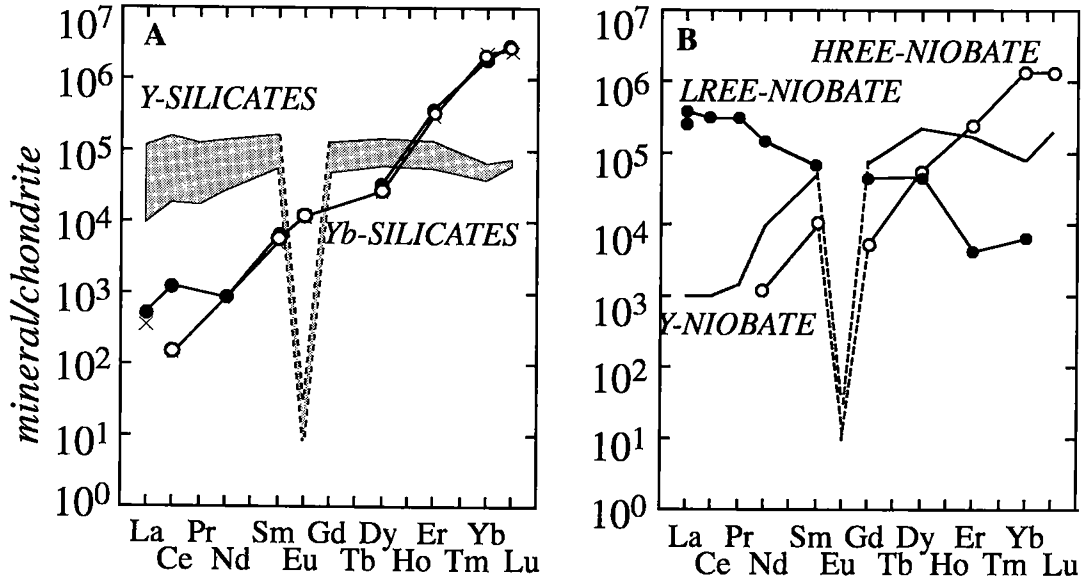

FIG. 4. A. Chondrite-normalized *REE* patterns of silicates and niobates. Grey area defined by several *REE*-patterns of Y-silicates. Superimposed patterns correspond to two selected Yb-silicates. B. Selected chondrite-normalized patterns of *LREE*, *HREE*, and Y-rich niobates.

TABLE 5. REPRESENTATIVE BULK COMPOSITION OF ALL THE ROCK TYPES FROM THE GALIÑEIRO COMPLEX

	Amphibole-biotite gneisses				*Aegirine-riebeckite gneisses*									*R-gneisses*							
					(Galiñeiro facies)			*(Magnetite facies)*			*(Zorro facies)*			*(R-1)*					*(R-2)*		
Samp.	ER-15	ER-23	ER-25	ER-30	ER110	ER-77	ER-80	ER-90	ER-3	ER46	ER-40	ER-7	ER-70	ER-57	S3-6	S3-13	S3-19	S4B4	S5B11	S7B-5	S6B-9
(wt.%)						*				*											
SiO_2	56.54	59.37	65.14	63.64	75.07	59.46	74.74	73.28	71.47	64.03	76.85	73.53	74.03	74.18	79.45	71.18	68.58	74.45	77.65	76.26	76.25
TiO_2	1.25	0.77	1.07	0.82	0.17	0.65	0.27	0.24	0.21	0.38	0.17	0.20	0.19	0.41	0.39	0.91	0.51	0.36	0.16	0.26	0.24
Al_2O_3	17.56	18.38	14.37	14.84	10.23	13.95	9.48	10.40	8.86	15.55	11.61	11.44	11.27	8.83	8.35	12.29	12.07	9.74	9.09	12.92	9.16
FeO	7.73	5.95	7.25	5.28	4.81	10.63	6.00	4.40	5.80	6.46	2.41	2.88	3.35	4.82	3.06	5.41	5.15	3.78	5.30	2.08	6.47
MgO	1.42	2.67	1.17	0.93	0.02	0.34	0.04	1.20	0.09	0.24	0.00	0.01	0.01	0.13	0.06	0.08	0.33	0.06	0.05	0.13	0.40
MnO	0.21	0.09	0.12	0.10	0.08	0.09	0.15	0.04	0.09	0.05	0.03	0.04	0.05	0.08	0.06	0.47	0.20	0.18	0.02	0.01	0.05
CaO	3.65	1.06	2.56	2.09	0.20	1.49	0.47	0.01	0.15	0.66	0.09	0.22	0.39	2.05	0.05	0.27	0.98	0.18	0.00	0.04	2.01
Na_2O	6.44	3.44	3.80	6.40	4.32	5.80	3.79	2.25	6.58	7.81	3.56	5.40	4.76	4.75	3.80	4.74	4.10	4.42	1.44	3.43	3.19
K_2O	3.06	7.62	3.83	5.15	4.57	1.73	3.54	3.83	5.72	2.19	5.01	5.93	5.10	0.16	0.18	1.00	2.60	3.23	4.87	4.11	0.38
P_2O_5	0.42	0.10	0.34	0.33	0.07	0.12	0.03	0.03	0.02	0.07	0.00	0.02	0.03	0.03	0.19	0.23	0.05	0.19	0.03	0.01	0.02
L.O.I	0.66	0.36	0.85	0.22	0.21	2.52	0.11	0.89	0.19	0.54	0.10	0.14	0.30	0.40	0.61	0.41	0.85	0.32	0.34	0.28	0.19
Total	98.94	99.81	100.50	99.80	99.75	96.78	98.62	96.57	99.18	97.98	99.83	99.81	99.48	95.84	96.20	96.99	95.42	96.91	98.95	99.53	98.36
												**	***								
CIPW normative components																					
Q	-	3.50	21.28	3.73	32.78	14.2	38.31	44.79	29.45	8.14	36.43	27.74	29.35	44.23	58.53	40.05	33.18	37.39	50.19	40.34	45.43
Or	18.31	45.12	22.62	30.46	27.06	10.74	21.17	23.59	34.06	13.23	29.64	35.10	30.33	0.99	1.11	6.10	16.2	19.70	29.10	24.44	2.22
Ab	54.82	29.17	32.13	47.71	27.23	51.58	29.40	19.84	13.83	67.57	30.16	25.87	29.76	41.99	33.50	41.38	36.57	33.15	12.32	29.21	26.63
An	10.1	4.62	10.47	-	-	6.95	-	-	-	0.93	0.45	-	-	2.40	-	-	4.78	-	-	0.13	9.43
Ne	0.20	-	-	-	-	-	-	-	-	-	-	-	-	-	-	-	-	-	-	-	-
Cm	-	2.79	0.13	-	-	0.12	-	2.66	-	-	0.17	-	-	-	1.98	3.52	0.89	-	1.47	2.80	-
Ac	-	-	0	5.73	7.75	-	2.69	-	9.40	-	-	4.64	5.42	-	-	-	-	4.80	-	-	-
Di	4.43	-	0	6.85	0.48	-	1.93	-	0.55	1.69	-	0.86	1.56	4.04	-	-	-	-	-	-	0.23
Hy	-	8.30	4.70	1.79	4.09	5.81	2.36	4.88	4.89	2.22	0.88	1.96	2.07	-	1.06	2.12	2.86	3.05	2.23	0.87	10.44
Ol	2.42	-	-	-	-	-	-	-	-	-	-	-	-	-	-	0	-	-	-	-	-
Il	2.40	1.47	2.03	1.56	0.32	1.3	0.52	0.48	0.40	0.74	0.32	0.38	0.36	0.81	0.77	1.78	1.02	0.71	0.31	0.50	0.45
Mag	6.31	4.80	5.84	1.39	-	9.00	3.54	3.69	-	5.32	1.94	-	-	4.06	2.57	4.50	4.37	0.74	4.32	1.69	5.14
Hem	-	-	-	-	-	-	-	-	-	-	-	-	-	-	-	-	-	-	-	-	-
Ap	1.01	0.24	0.80	0.78	0.17	0.30	0.07	0.07	0.05	0.17	-	0.05	0.07	0.07	0.47	0.56	0.12	0.46	0.07	0.02	0.05
ITT	73.33	77.79	76.03	81.90	87.06	76.53	88.89	88.21	77.35	88.93	96.2	88.71	89.44	87.21	93.14	87.52	85.94	90.24	91.61	93.99	74.27
AI	0.79	0.76	0.723	1.085	1.178	0.82	1.06	0.75	1.92	0.98	0.97	1.34	1.18	0.91	0.77	0.72	0.79	1.11	0.84	0.78	0.62

* Anomalous samples, excluded from statistics. TTI=Differentiation Index. ** Contains 3.41% of Na metasilicate. *** contains 1.07% of Na metasilicate.

TABLE 6. REPRESENTATIVE TRACE ELEMENT CONCENTRATIONS OF ALL THE ROCK TYPES FROM THE GALIÑEIRO COMPLEX

	Amph.-biotite gneisses				*Aegirine-riebeckite gneisses*									*R-gneisses*							
					(Galiñeiro facies)			*(Magnetite facies)*			*(Zorro facies)*			*(R-1)*					*(R-2)*		
Samp.	ER15	ER23	ER25	ER30	ER11 0	ER-77	ER-80	ER-90	ER-3	ER-46	ER-40	ER-7	ER-70	ER-57	S3-6	S3-13	S3-19	S4B-4	S5B11	S7B-5	S6B-9
(ppm)						*				*											
Li	33	69	15	71	56	77	100	18	57	62	39	24	48	4.0	-	16	16	3.6	16	11	16
Rb	110	187	157	238	385	205	311	381	367	238	203	229	229	11	3.6	98	165	168	539	256	76
Cs	6.8	11	5.4	11	0.9	1.3	2.7	1.9	1.2	1.5	2.4	2.3	3.7	1.1	2.1	16	9.6	17	1.2	0.7	2.6
Be	8.0	2.7	2.6	6.1	4.8	1387	9.2	5	6.8	356	3.4	4.7	6.4	4.4	27	12	14	28	4.2	7.9	2.9
Sr	321	110	245	179	5.1	49	28	9.8	6.6	24	1.2	7.4	9.2	125	30	31	64	37	7.0	13	93
Ba	890	1041	1026	636	4.7	14	17	25	2.2	16	21	29	22	27	23	40	41	94	12	35	15
Cr	16	102	57	33	81	-	83	69	108	32	110	96	95	90	510	376	280	91	95	65	88
Co	8.0	15	9.0	5.5	0.5	0.5	0.8	0.6	1.7	0.2	0.7	0.7	1.4	0.5	2.5	2.7	1.7	0.6	0.7	0.5	4.4
Ni	-	51	4.4	-	-	-	-	-	5.0	-	-	-	278	-	4.2	-	11	0.7	2.2	-	2.6
Cu	10.2	13	6.0	5.0	2.86	14	2.8	1.9	0.1	3.4	0.8	2.9	226	72	139	77	17	87	29	9.4	399
Zn	86	81	108	89	190	366	281	234	260	231	109	151	303	259	1163	1866	1077	1488	78	109	682
Ga	19	16	18	20	37	49	39	40	46	51	33	33	35	50	45	50	39	49	37	37	39
Y	45	17	54	60	80	8447	194	483	95	2658	15	63	72	692	2420	1812	2237	1309	117	300	274
Nb	92	20	59	70	237	733	251	445	293	362	97	187	109	2746	2127	2157	1020	1573	228	344	594
Ta	12	2.7	7.2	8.3	25	91	26	44	16	58	12	21	10	322.8	108	148	80	203	26	42	71
Zr	250	178	318	364	1178	1206	2038	1509	1811	1343	262	662	426	8584	6224	7628	2746	8134	1080	1287	4437
Hf	4.7	2.5	6.1	11	15	26	52	35	42	23	5.5	6.1	3.4	227	102	115	71	40	13	15	99
Mo	2.5	0.2	1.2	12	3.3	1.5	4.1	20	30	1.6	2.7	2.4	3.4	20	25	31	6.4	1.6	66	24	606
Sn	14	2.5	5.1	11	19	65	24	45	4.3	40	7.8	14	12	132	53	64	52	27	59	32	17
Tl	0.5	0.8	0.5	0.9	1.0	0.5	0.7	1.0	0.5	0.7	0.5	0.6	0.5	-	0.1	0.5	0.4	0.6	0.6	0.4	0.4
W	9.2	4.0	5.5	3.9	6.1	50	6.2	8.3	7.3	25	7.3	6.4	5.1	72	41	31	23	26	9.6	7.6	12
Pb	-	-	-	2.6	2.4	235	-	-	94	95	-	25	53	1828	339	552	180	347	-	-	140
U	3.6	2.0	3.4	4.3	12	77	25	23	5.2	49	3.4	7.5	5.2	166	153	183	66	114	8.5	18	48
Th	13	14	13	20	63	7223	18	30	42	4923	15	41	18	101	1369	220	823	654	29	59	159
F	1606	674	1147	5510	1174	7509	4888	1025	2046	6996	-	52	3916	26042	930	1835	4753	1687	106	525	21287

* Anomalous samples, excluded from statistics. - below detection limit.

TABLE 7. REPRESENTATIVE REE CONCENTRATIONS OF ALL THE ROCK TYPES FROM THE GALIÑEIRO COMPLEX

	Amphibole-biotite gneisses				*Aegirine-riebeckite gneisses*									*R-gneisses*							
					(Galiñeiro facies)			*(Magnetite facies)*			*(Zorro facies)*			*(R-1)*					*(R-2)*		
Samp.	ER15	ER23	ER25	ER30	ER110	ER77	ER80	ER-90	ER-3	ER46	ER40	ER7	ER70	ER-57	S3-6	S3-13	S3-19	S4B-4	S5B11	S7B-5	S6B-9
(ppm)						*				*											
La	81	43	41	69	174	175	359	603	776	69	15	70	150	961	1088	1700	880	830	229	250	569
Ce	134	92	117	147	337	778	572	693	975	300	31	141	216	1820	2377	3884	2013	1928	479	497	1120
Pr	18	10	11	16	43	123	83	143	117	37	3.5	17	35	200	284	472	245	243	63	60	134
Nd	69	38	46	59	163	563	308	549	248	163	28	62	133	623	1004	1692	895	907	262	217	493
Sm	12	7.0	10	12	30	249	60	118	43	71	5.1	14	26	133	251	399	213	212	57	50	92
Eu	4.1	1.5	2.4	2.1	0.9	14	2.6	4.7	1.6	3.9	0.0	0.5	0.9	6.0	11	17	10	9.0	2.4	2.7	3.2
Gd	10	5.6	9.2	10	20	308	49	104	20	92	2.7	12	19	142	235	339	208	178	48	48	68
Tb	1.4	0.6	1.4	1.6	2.9	118	7.6	18	2.5	35	0.4	2.3	2.7	27	55	62	51	36	6.3	9.3	10
Dy	8.4	3.7	9.6	10	17	1200	41	102	17	347	3.2	15	14	150	386	376	361	230	28	58	50
Ho	1.7	0.7	2.0	2.0	3.4	421	7.7	21	3.3	115	0.6	3.1	2.4	28	91	78	81	53	4.8	12	10
Er	4.7	1.6	5.5	5.7	10	2351	19	51	8.2	595	1.9	8.3	6.5	61	248	190	209	149	11	32	30
Tm	0.7	0.2	0.8	0.9	1.8	1050	2.7	6.9	1.2	246	0.3	1.4	0.9	8.2	35	24	27	24	1.5	4.8	4.9
Yb	4.8	1.4	5.0	5.4	11	8797	15	36	6.6	2494	2.2	8.9	5.7	40	151	114	108	124	9.6	27	30
Lu	0.6	0.2	0.6	0.7	1.5	1661	2.1	4.5	0.8	381	0.4	1.1	0.7	4.7	17	14	11	15	1.3	3.5	4.0
LaN/LuN	13.60	25.14	7.00	9.82	12.75	0.01	18.12	14.24	102.75	0.02	4.73	6.57	22.31	21.62	6.93	12.87	8.75	5.92	18.78	7.65	15.14
EuN/Eu*	0.74	0.71	0.75	0.58	0.10	0.15	0.15	0.13	0.17	0.15	0.00	0.13	0.12	0.13	0.14	0.14	0.14	0.14	0.14	0.17	0.13

* Anomalous samples, excluded from statistics.

WHOLE-ROCK CHEMISTRY

Sixty-six samples representing all Galiñeiro rock types were analyzed for major and the following trace elements: Li, Rb, Cs, Be, Sr, Ba, Cr, Co, Ni, Cu, Zn, Ga, Y, Nb, Ta, Zr, Hf, Mo, Sn, Tl, W, Pb, Th, U, F and La, Ce, Pr, Nd, Sm, Eu, Gd, Tb, Dy, Ho, Er, Tm, Yb and Lu. Compositions of selected samples are presented in Tables 5, 6, and 7.

Major elements

Aegirine – riebeckite gneisses have SiO_2 in the range 70–75 wt.%, an agpaitic index (AI = mol [Na_2O + K_2O]/Al_2O_3) close to 1 (average AI = 1.02), with Fe/[Fe + Mg] ≈ 0.96, $Na_2O + K_2O \approx 8$ wt.%, $Na_2O/K_2O \approx 1$, and low Al_2O_3, CaO and MgO contents (Table 5). Amphibole – biotite gneisses have a lower agpaitic index (0.7 < AI < 1.01), Fe/[Fe + Mg] ≈ 0.7, $Na_2O + K_2O = 8.5$ wt.%, $Na_2O/K_2O \approx 1.1$ and moderately elevated Al_2O_3, CaO, and MgO contents. The major-element composition of the R–2 gneisses is very close to that of aegirine – riebeckite gneisses, but some specimens have significantly lower K_2O contents and higher AI. This tendency is still more marked in R–1 gneisses, which show a marked depletion in K_2O and a slight enrichment in MnO, TiO_2, and P_2O_5.

HFSE and REE

The abundance of rare earths and high-field-strength elements in the Galiñeiro rocks (Tables 6 and 7) increases according to the following sequence: (1) amphibole – biotite gneisses, (2) Zorro facies, (3) Galiñeiro facies, (4) Magnetite facies, (5) R–2 gneisses, and (6) R–1 gneisses, the latter showing accumulations of *REE* and *HFSE* of economic value. Some samples from the Galiñeiro and Magnetite facies also show enrichments comparable to those of R–1 gneisses. The rare-earth and high-field-strength elements do not show any correlation with major elements other than a weak negative one with potassium. Zr shows an excellent positive correlation with Nb, Ta, and U but, surprisingly, not with Hf. The Zr:Hf ratio for most samples is 40–50, close to the terrestrial ratio, but some samples, mostly of R–1 gneisses, have Zr/Hf values as high as 200–300, which do not correlate with any other geochemical variable, although they always occur in low-Y samples. Concentrations of Y, Th, and rare-earth elements also increase with Zr, but the correlation is not as good as with Nb, Ta, and U, especially at high concentrations. Th:U ratios are quite variable, but in general close to 7. Some samples from aegirine – riebeckite gneisses, especially from the Galiñeiro or Magnetite facies, however, have a tremendous enrichment in Th (≈ 5000–7000 ppm), with Th/U ≈ 100. These samples are simultaneously enriched in Be (≈ 1400 ppm), Y (≈ 8500 ppm), and the heavy rare-earth elements (*e.g.*, Dy ≈ 1200 ppm, Yb ≈ 8800 ppm).

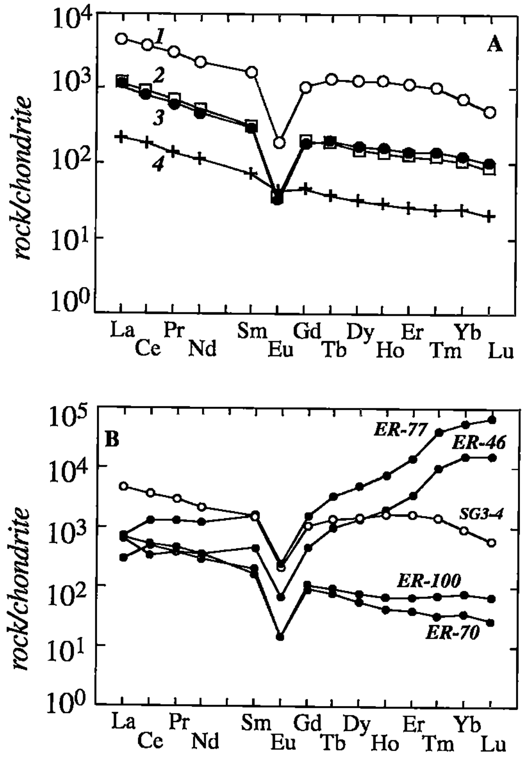

Fig. 5. A. Chondrite-normalized *REE* patterns of average whole-rock samples for every rock-type of the Galiñeiro complex: (1) R–1 gneisses, (2) R–2 gneisses, (3) aegirine – riebeckite gneisses, (4) amphibole – biotite gneisses. Anomalous samples have been excluded. B. Selected *REE*-patterns of representative "normal" samples (ER–70 and ER–100 from Zorro and Galiñeiro facies, respectively) and anomalous samples (ER–77, ER–46 from Galiñeiro and Magnetite facies and SG3–4 from R–1 gneisses).

The concentration of rare-earth elements is high in all facies, with average Σ*REE* of 280 ppm in amphibole – biotite gneisses, 1100 ppm in aegirine – riebeckite gneisses (anomalous samples excluded), 1300 ppm in R–2 gneisses and 5500 ppm in R–1 gneisses (Table 7). Chondrite-normalized *REE* patterns of amphibole – biotite gneisses show a smooth, constant decrease from La (≈ 200 × chondrite), to Lu (≈ 20 × chondrite), with a small negative Eu anomaly (Eu/Eu* ≈ 0.75) (Fig. 5A). Aegirine – riebeckite gneisses have a similar *LREE/HREE* fractionation, with La_N/Lu_N ≈ 11 (although with notable exceptions, see Table 7), but show a steep negative Eu anomaly (Eu/Eu* ≈ 0.10). Chondrite-normalized *REE* patterns of R–2 gneisses are very similar to those of aegirine – riebeckite gneisses (La_N/Lu_N ≈ 15.5; Eu/Eu* ≈ 0.1 – 0.2). Chondrite-normalized *REE* patterns of R–1 gneisses, however, show a marked convexity between Gd and Lu (Fig. 5A). The above-mentioned samples, anomalously enriched in Y, Th, and Be, also have anomalous chondrite-normalized *REE* patterns, with a positive slope, moderate from La to Sm, but steep from Gd to Lu, and with a strong Eu anomaly (samples ER–46 and ER–77 in Fig. 5B).

Trace elements other than HFSE and REE

Li contents are highly variable within the same facies (Table 6). On average, however, they increase from amphibole – biotite gneisses (~55 ppm Li) to aegirine – riebeckite gneisses (~61 ppm) and then decrease to R–2 (~25 ppm) and to R–1 (~8 ppm) gneisses. Rb is more uniform for all rock types (~270 ppm Rb) except for R–1 gneisses, which contain ~80 ppm. The concentration of Be is extremely variable. It is usually on the order of a few ppm, but samples ER–46 and ER–77 have 360 and 1390 ppm, respectively. The level of Sr and Ba is, in general, very low, decreasing from amphibole – biotite gneisses (~225 ppm Sr, ~785 ppm Ba) to aegirine – riebeckite gneisses (~14 ppm Sr, ~20 ppm Ba) and to R–2 and R–1 gneisses (~45 ppm Sr, ~60 ppm Ba). R–1 gneisses, and to a lesser extent R–2 gneisses, also show a remarkable enrichment in Zn, Ni, Cu, Pb, and Mo (Table 6), thus reflecting the presence of accessory sulfides, especially sphalerite. Ga increases from ~20 ppm in amphibole – biotite gneisses to ~35 ppm in R–2 gneisses, ~40 ppm in aegirine – riebeckite gneisses and ~45 ppm in R–1 gneisses.

Fluorine

Fluorine concentration is invariably very high, increasing gradually from ampibole – biotite gneisses (F ≈ 0.18 wt.%) to R–1 gneisses (0.5 < F < 2 wt.%). There is no clear correlation between the concentration of fluorine and that of any other element.

ISOTOPE GEOCHEMISTRY AND GEOCHRONOLOGY

Isotopic studies on Galiñeiro rocks reveal a complicated picture that probably reflects the long postmagmatic history of these rocks. Rb–Sr systematics on eight whole-rock samples from aegirine – riebeckite and R-gneisses gave an isochron age of 325 ± 19 Ma (Fig. 6A) with initial $^{87}Sr/^{86}Sr = 0.737575 \pm 0.054$ (2σ) (Table 8, see also Montero 1993). Sm–Nd systematics for four whole-rock samples gave an isochron age of 541 ± 81 Ma (Fig. 6B) and an initial $^{143}Nd/^{144}Nd = 0.512051 \pm 0.0000648$ (2σ). U–Pb on zircon concentrates gave two concordant ages, one about 310 Ma and the other about 370 Ma (Fig. 7A). Finally, $^{207}Pb/^{206}Pb$ determinations on eight single crystals of zircon gave an age of 460 ± 22 Ma (Fig. 7B).

TABLE 8. ISOTOPIC RATIOS OF SELECTED SAMPLES FROM THE GALIÑEIRO COMPLEX, SPAIN

	$^{87}Rb/^{86}Sr$	$^{87}Sr/^{86}Sr$	$^{147}Sm/^{144}Nd$	$^{143}Nd/^{144}Nd$	$^{207}Pb/^{235}U$	$^{206}Pb/^{238}U$	$^{207}Pb/^{206}Pb$
ER-57	0.248	0.71150	0.1285	0.51251	0.3609	0.04856	.
SG3-14	7.079	0.76473	0.1384	0.51254	.	.	.
ER-3	161.885	1.48497	0.1047	0.51242	0.3512	0.04825	.
ER-90	112.061	1.20672	.	.	.	.	.
ER-110	218.851	1.74619	0.1122	0.51244	0.4454	0.05956	.
ER-80	32.728	0.88100	.	.	.	.	.
ER-70	72.740	1.17185	.	.	.	.	.
ER-40	489.616	3.00538	.	.	0.4402	0.05885	0.56190 *

Samples from Aegirine-riebeckite and R-gneisses: ER-57 and SG3-14 from R-1 gneisses, ER-3 and ER-90 from Magnetite facies, ER-110 and ER-80 from Galiñeiro facies and ER 70 and ER-40 from Zorro facies. U-Pb ratios determined in zircon concentrates. $^{207}Pb/^{206}Pb$ ratios determined in zircon single grains: * is the mean of eight different grains.

The interpretation of these data is not simple, but we tentatively suggest that:

(1) The 460 ± 22 Ma age from $^{207}Pb/^{206}Pb$ data obtained on a single grain of zircon probably reflects the age of crystallization of the magmas that formed the Galiñeiro pluton. This age is in good agreement with data obtained in other peralkaline rocks in the area [486 ± 24 Ma: Priem *et al.* (1966); 469 ± 8 Ma: Kuijper (1979)] and is within the error range of the Sm–Nd isochron.

(2) The U–Pb concordant age of zircon around 370 Ma may reflect the reactivation of the peralkaline rocks during the first important phase of Hercynian deformation (Ferreira *et al.* 1987).

(3) The second concordant zircon age and Rb/Sr ages (310 Ma) could reflect the peak of the Hercynian metamorphism, which produced a massive generation of crustal granites in the Central Iberian Zone, with ages ranging from 320 to 300 Ma (Serrano Pinto *et al.* 1988). Metamorphic recrystallization of the feldspars caused the breakdown of the isotopic Rb–Sr system, and led to the total recrystallization of the rock at low-pressure amphibolite-facies conditions (Floor 1974).

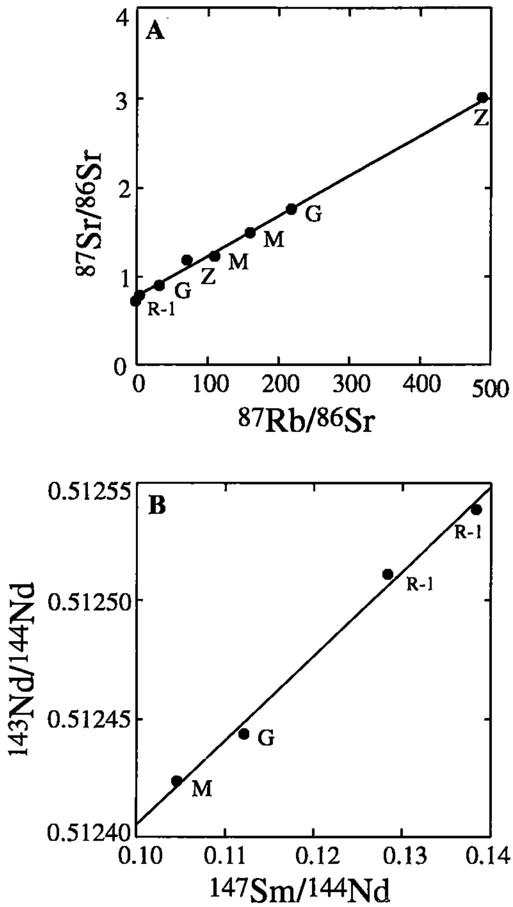

FIG. 6. A. Rb/Sr isochron for eight whole-rock samples from the Galiñeiro complex. Initial $^{87}Sr/^{86}Sr = 0.737578 \pm 0.054$ (2σ). Isotopic age: 325 ± 19 Ma. B. Sm/Nd isochron for four whole-rock samples. Initial $^{143}Nd/^{144}Nd = 0.512051 \pm 0.000064$ (2σ)· Isotopic age: 541 ± 81 Ma., ε^{481}_{CHUR}(ND) = +1.5 (Z, M, G: Zorro, Magnetite and Galiñeiro facies, respectively; R–1: R–1 gneisses).

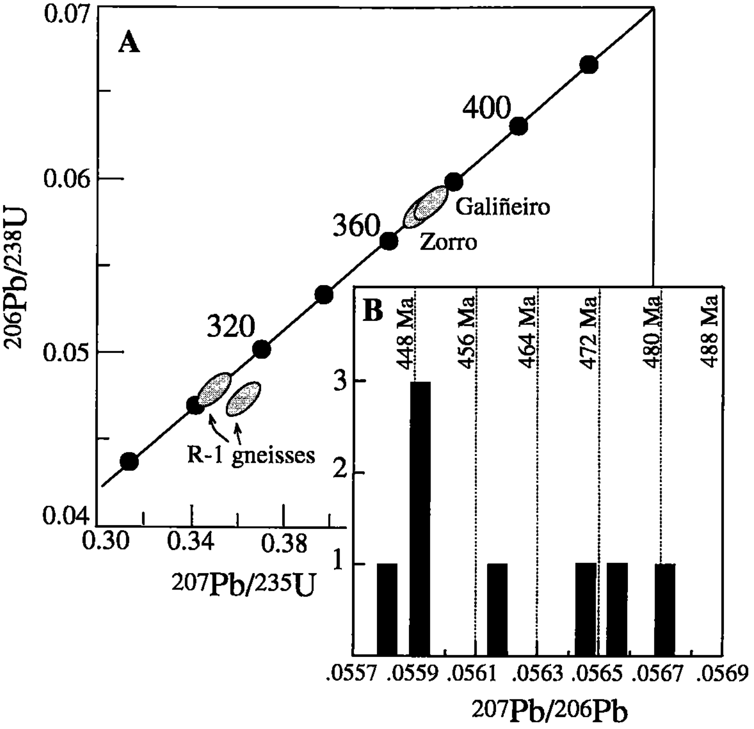

FIG. 7. A. U/Pb concordia diagram for zircon concentrates in four samples from the Galiñeiro complex with two concordant ages (about 310 and 370 Ma). B. Histogram of ^{207}Pb/^{206}Pb values in eight single grains of zircon from the Zorro facies, whose mean value (0.056190) corresponds to a radiogenic age of 460 ± 22 Ma.

DISCUSSION

Petrogenesis

The mineralogy and geochemical signature of the Galiñeiro rocks most likely correspond to "early anorogenic" (Bonin 1990) A-type granites. On the discrimination diagrams for granites of Whalen *et al.* (1987), aegirine – riebeckite and R-gneisses systematically plot in the field of A-type granites; only some amphibole – biotite gneisses plot in the area corresponding to orogenic granites (Fig. 8A). In addition, the low Yb/Ta, very low Y/Nb, and Zr/Nb < 10 shown by the aegirine – riebeckite gneisses (Fig. 8B) suggest that they were A1-type granites, considered to represent mantle differentiates emplaced during continental rifting processes or intraplate magmatism (Eby 1990, 1992). Since this idea is consistent with Nd isotope data [$\varepsilon_{CHUR}{}^{481}$(Nd) = +1.5], we suggest that the magmas that produced the Galiñeiro complex had a mantle source, ruling out partial melting of residual felsic lower crust (Pin *et al.* 1992, Montero 1993), and probably consisted of volatile-rich alkaline basaltic melts evolving by crystal fractionation through the critical plane of silica saturation (Coombs trend: Miyashiro 1978), producing an intermediate member represented by amphibole – biotite gneisses and residual liquids with an alkali rhyolite composition represented by the aegirine – riebeckite gneisses.

Several peralkaline granites and peralkaline rhyolites with ages from 423 to 470 Ma and a chemical composition roughly similar to that of Galiñeiro (though not so enriched in rare-earth and high-field-strength elements) occur within a broad belt in Spain and Portugal: the Malpica – Tuy unit (Gil Ibarguchi & Ortega 1985), Tras-os-Montes (Ribeiro 1987), Portalegre, and the Badajoz – Córdoba zone (García Casquero *et al.* 1985). Taking into account the close relationship between peralkaline felsic activity and extensional tectonics (*e.g.*, Bonin 1990), we suggest that Galiñeiro and similar Iberian rocks were generated during an ensialic extension event in the early

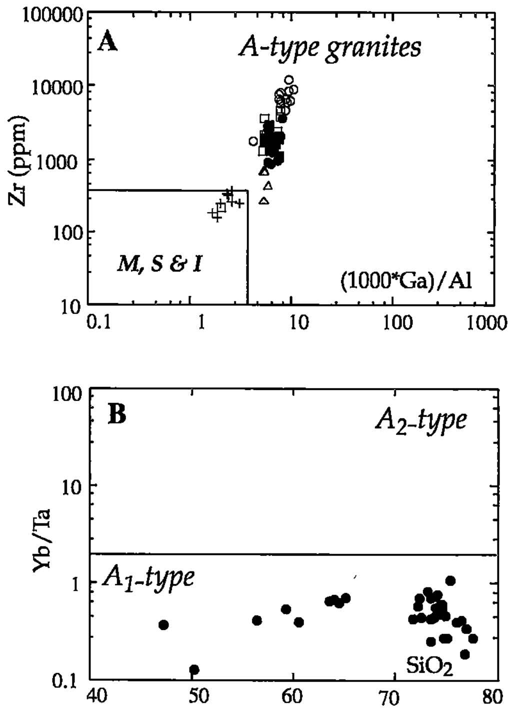

FIG. 8. A. Discrimination diagram for A-type granites (Whalen *et al.* 1987) for the Galiñeiro rocks. Crosses: amphibole – biotite orthogneisses, black dots: Galiñeiro facies, black squares: Magnetite facies, white triangles: Zorro facies, white dots: R-gneisses. B. Discrimination diagram for A-type granites, showing the fields of subtypes A_1 and A_2 (Eby 1992), and the distribution of points for the Galiñeiro rocks (R-gneisses excluded).

Ordovician (Pin & Marini 1993), probably as a consequence of the separation of eastern Avalonia from Gondwana (Prigmore *et al.* 1997).

Mobility of major and trace elements during late- and post-magmatic stages

Many of the most significant geochemical anomalies exhibited by the Galiñeiro complex, such as the decoupling of Zr and Hf or of Th and U, the high spatial variability and extreme local enrichment of trace elements, as well as the K and Rb depletion of R-gneisses, cannot be explained by any known magmatic process or combination of processes. These features, together with the elevated fluorine contents and the existence of associations of exotic *REE*-rich and *HFSE*-rich minerals, suggest that during the last stages of magmatic crystallization, fluids enriched in the rare-earth and high-field-strength elements, fluoride, sulfide, and carbonate anions were released, thus producing the redistribution of *REE* and *HFSE* in aegirine – riebeckite gneisses and country rocks. These fluids, where channeled through faults or cracks, caused the strong metasomatic alteration which led to the R-gneisses. Similar phenomena have been described in syenite pegmatites from the Oslo region, Norway (Larsen 1996), the Thor Lake *REE*–Y–Be deposits, Northwest Territories (Taylor & Pollard 1996), and amazonitic pegmatites and metasomatic bodies related to the West Keivy peralkaline granite, Kola Peninsula, Russia (Belolipetskii & Voloshin 1996). These phenomena have always been interpreted as being a result of late- or post-magmatic metasomatic processes involving fluids emanating from peralkaline intrusions.

Some important aspects of the behavior of these metasomatic fluids may be revealed by the joint study of zircon morphology and Zr solubility in melts. Calculations of Zr solubility using the experimental model of Watson & Harrison (1983) indicate that melts with the same Zr and major-element composition as the Galiñeiro rocks become saturated in Zr at 1000–1100°C. However, the morphology of the zircon crystals indicates that massive crystallization of zircon only took place at temperatures as low as ~600°C (see above), thus indicating that Zr was in some way stabilized within the melt. Given the high alkalinity and F contents of the melt, it is probable that the formation of zirconium–fluoride complexes (Collins *et al.* 1982, Dietrich 1968, Watson 1979, Watson & Harrison 1983), stable at high temperatures and very soluble (Ferguson 1974), could have contributed to the stabilization of Zr within the melt (Keppler 1993; but see Farges 1996). These complexes likely remained stable until the last stages of crystallization, when the combined effects of decreasing temperature and decreasing F activity, possibly related to the formation of F-rich biotite and amphibole, decreased the activity of fluoride in the melt, thereby causing the breakdown of complexes (Collins *et al.* 1982) and releasing Zr, which precipitated as low-temperature zircon. Apart from fluorine, other ligands such as carbonates, phosphates, *etc.* (Bilal *et al.* 1978, Wendlandt & Harrison 1979, Wood 1990a, b) may have helped to stabilize the trace elements, especially the rare-earth elements, down to relatively low temperatures within the fluid phase.

The strong decoupling of Zr–Hf, U–Th, *LREE–HREE*, as well as the anomalous local enrichments in some elements, however, can scarcely be explained by the action of a single episode of metasomatism, suggesting instead the action of fluids with very different compositions, probably acting at different times in the history of Galiñeiro. Taking into account the high F and CO_2 contents of the Galiñeiro rocks, it is logical to suppose that once the original melts had completely crystallized, any further input of energy, even a moderate one, may have caused appreciable mobilization of fluids with variable metasomatic capability, depending on the activity of ligands and temperature. The variety of ages produced by isotopic systems (see above), and the presence of veinlets of secondary monazite, thorite, bastnäsite and zircon are all consistent with that idea, and suggest that the Galiñeiro system was repeatedly re-activated during its postmagmatic history, especially during the Hercynian episode of metamorphism.

CONCLUSIONS

Rocks from the Galiñeiro orthogneissic complex crystallized from magmas ultimately derived from a mantle source. The original magma most likely had the composition of a volatile-rich alkali basalt that evolved by crystal fractionation and followed a Coombs-type trend whose end product (alkali rhyolite) now is represented by the peralkaline orthogneisses. The emplacement of magmas occurred at high levels in the crust at 480–460 Ma during a extensional tectonic regime (possibly continental rifting). Magmatic fractionation produced residual fluids extremely enriched in ligands, especially fluorine, able to complex the rare-earth and high-field-strength elements. The decrease of the activity of fluorine in fluids related to decreasing temperature and the crystallization of F-bearing major minerals produced the breakdown of such complexes, releasing the rare-earth and high-field-strength elements, which then precipitated *REE*-rich and *HFSE*-rich minerals such as bastnäsite, monazite, xenotime, fergusonite – formanite, aeschynite, samarskite, betafite, allanite, thalenite – yttryalite, titanite, zircon, thorite, *etc*., either isolated or, more commonly, forming associations of intricate fine-grained aggregates. These fluids produced endo- and exo-metasomatism of the Galiñeiro complex, and, where they circulated through channels and cracks, produced the R-gneisses.

The elevated contents of fluorine, CO_2 and sulfide of the Galiñeiro system, together with the energy inputs related to different phases of the Hercynian metamorphism, caused episodic metasomatic mobilization, reflected by the concordant U–Pb ages at 370 and 310 Ma measured on zircon. The development of low-temperature minerals and veins of secondary monazite, thorite, bastnäsite, and zircon probably account for the exotic geochemical features (*e.g*., Zr/Hf > 100, enriched Be, Th, and heavy rare-earth elements) of some samples. Hercynian deformation and metamorphism also caused the recrystallization of the major mineral assemblage at intermediate to low temperatures (less than 550°C) and intermediate pressures (0.5–0.6 GPa).

ACKNOWLEDGEMENTS

The authors thank F. Bea and G. Fershtater for the critical reading of the manuscript and fruitful comments, N. Eby for his A-type granite data-base and his help, L. Villa for his aid in the field and laboratory work, Y. Ronkin for isotopic determinations, G. Garuti, F. Zaccarini and G. Nagy for their help with electron-microprobe analyses of accessory minerals. The authors also express their gratitude to D.M. Shaw, B. Bonin, G.T. Nixon, J.M. Hanchar and R.F. Martin for their helpful revisions, which greatly contributed to improve the manuscript. Christine Laurin is also thanked for improving the English. This work has been financially supported by the Project ERCROS S.A. Mining Company – Univ. Oviedo N° A4–025–88 and by the Spanish Interministry Commission for Science and Technology (CICYT), projects GEO89–0600–CO3–02 and AMB93–0535.

REFERENCES

ARENAS, R., FARIAS, P., GALLASTEGUI, G., GIL IBARGUCHI, J.I., GONZÁLEZ LODEIRO, F., KLEIN, E., MARTÍN PARRA, L.M., MARTÍNEZ CATALÁN, J.R., ORTEGA, E., DE PABLO MACÍA, J.G., PEINADO, M. & RODRÍGUEZ FERNÁNDEZ, L.R. (1988): Características geológicas y significado de los dominios que componen la zona de Galicia Tras-Os-Montes. *II Congreso Geológico de España (Granada)*, 75-84.

ARRIBAS, A. (1963): Mineralogía y metalogenia de los yacimientos españoles de uranio: Porriño, Pontevedra. *Bol. R. Soc. Esp. Hist. Nat.* (*G*) **61**, 51-75.

BEA, F. (1996): Residence of REE, Y, Th, U in granites and crustal protoliths. Implications for the chemistry of crustal melts. *J. Petrol.* **37**, 521-552.

________, MONTERO, P., STROH, A. & BAASNER, J. (1996): Microanalysis of minerals by Excimer UV–LA–ICP–MS system. *Chem. Geol.* **133**, 145-156.

BELKOV, I.V. (1979): *The Accessory Minerals of Granitoids of the Kola Peninsula.* Science Press, Leningrad, Russia (in Russ.).

________, BATIEVA, I.D., VINOGRADOVA, G.V. & VINOGRADOV, A.N. (1988): *Mineralization and Fluid Regime of Contact Zone of the Intrusion of the Alkaline Granite.* USSR Academy of Sciences, Apatity, Russia (in Russ.).

BELOLIPETSKII, A.P. & VOLOSHIN, A.V. (1996): Yttrium and rare earth element minerals of the Kola Peninsula, Russia. *In* Rare-Earth Minerals, Chemistry, Origin and Ore Deposits (A.P. Jones, F. Wall & C.T. Williams, eds.). The Mineralogical Society Series **7**. Chapman & Hall, London, U.K.

BILAL, B.A., HERRMANN, F. & FLEISCHER, W. (1978): Potentiometric study of fluoro complexes of rare earth elements in fluorite bearing model systems. *J. Inorg. Nucl. Chem.* **41**, 347-350.

BONIN, B. (1990): From orogenic to anorogenic settings: evolution of granitoid suites after major orogenesis. *Geol. J.* **25**, 261-270.

COLLINS, W.J., BEAMS, S.D., WHITE, A.J.R. & CHAPPELL, B.W. (1982): Nature and origin of A-type granites with particular reference to southeastern Australia. *Contrib. Mineral. Petrol.* **80**, 189-200.

DIETRICH, R.V. (1968): Behavior of zirconium in certain artificial magmas under diverse P–T conditions. *Lithos* **1**, 20-29.

DRAKE, M.J. & WEILL, D.F. (1972): New rare earth element standards for electron microprobe analysis. *Chem. Geol.* **10**, 179-181.

EBY, N.G. (1990): The A-type granitoids: a review of their occurrence and chemical characteristics and speculations on their petrogenesis. *Lithos* **26**, 115-134.

________ (1992): Chemical subdivision of the A-type granitoids: petrogenetic and tectonic implications. *Geology* **20**, 641-644.

FARGES, F. (1996): Does Zr–F "complexation" occur in magmas? *Chem. Geol.* **127**, 253-268.

FARIAS, P., GALLASTEGUI, G., GONZÁLEZ LODEIRO, F., MARTÍNEZ, J., MARTÍN PARRA, L.M., MARTÍNEZ CATALÁN, J.R., DE PABLO MACÍA, J.G., & RODRÍGUEZ FERNÁNDEZ, L.R. (1987): Aportaciones al conocimiento de la litoestratigrafía y estructura de Galicia Central. *Mem. Lab. Mineral. Geol., Fac. Ciencias de Porto* **1**, 411-431.

FERGUSON, J.E. (1974): *Stereochemistry and Bonding in Inorganic Chemistry.* Prentice Hall, Englewood Cliffs, New Jersey.

FERREIRA, N., IGLESIAS, M., NORONHA, F., PEREIRA, E., RIBEIRO, A. & RIBEIRO, M.L. (1987): Granitoides da zona Centro-Ibérica e seu enquadramento geodinâmico. *In* Geología de los granitoides y rocas asociadas del Macizo Hespérico (F. Bea, A. Carnicero, J.C. Gonzalo, M. López Plaza & M.D. Rodríguez Alonso, eds.). Ed. Rueda, Madrid, Spain (37-51).

FLOOR, P. (1966): Petrology of an aegirine-riebeckite gneiss-bearing part of the Hesperian Massif: the Galiñeiro and surrounding areas, Vigo, Spain. *Leidse Geol. Meded.* **36**, 1-204.

________ (1974): Alkaline gneisses. *In* The Alkaline Rocks (H. Sørensen, ed.). John Wiley & Sons, London, U.K. (124-142).

FÖRSTER, H.J. (1993): U–Th–Y–REE-bearing accessory minerals in Hercynian granites of the Erzgebirge (Ore Mountains), Germany. *Geol. Soc. Am., Abstr. Programs* **25**, A42-A43.

________ & RHEDE, D. (1995): Extreme compositional variability in granitic monazites. *Third Hutton Symposium on the Origin of Granites and Related Rocks (College Park, Maryland)* (M. Brown & P.M. Piccoli, eds.). *U.S. Geol. Surv., Circ.* **1129**, 54-55.

GARCÍA CASQUERO, J.L., BOELRIJK, N.A.I.M, CHACÓN, J. & PRIEM, H.N.A. (1985): Rb–Sr evidence for the presence of Ordovician granites in the deformed basement of the Badajoz-Córdoba belt, SW Spain. *Geol. Rundsch.* **74**(2), 379-384.

GIL IBARGUCHI, J.I. & ORTEGA GIRONÉS, E. (1985): Petrology, structure and geotectonic implications of glaucophane-bearing eclogites and related rocks from the Malpica – Tuy (MT) Unit, Galicia, northwest Spain. *Chem. Geol.* **50**, 145-162.

JACKSON, J.N., DRYSDALL, A.R. & STOESER, D. (1985): Alkali granite-related Nb–Zr–REE–U–Th mineralization in the Arabian Shield. *In* High Heat Production (HHP) Granites, Hydrothermal Circulation and Ore Genesis. The Institute of Mining and Metallurgy, London, U.K. (479-487).

KEPPLER, H. (1993): Influence of fluorine on the enrichment of high field strength trace elements in granitic rocks. *Contrib. Mineral. Petrol.* **114**, 479-488.

KUIJPER, R.P. (1979): *U–Pb Systematics and the Petrogenetic Evolution of Infracrustal Rocks in the Paleozoic Basement of Western Galicia (NW Spain).* Ph.D. thesis, Verhandeling nr 5 Zwo Laboratorium voor isotopen-Geologie, Amsterdam, The Netherlands.

LARSEN, A.O. (1996): Rare-earth minerals from the syenite pegmatites in the Oslo region, Norway, *In* Rare Earth Minerals, Chemistry, Origin and Ore Deposits (A.P. Jones, F. Wall & C.T. Williams, eds.). The Mineralogical Society Series **7**. Chapman & Hall, London, U.K.

MARIANO, A.N. (1989): Economic geology of rare earth elements. *In* Geochemistry and Mineralogy of Rare Earth Elements (B.R. Lipin & G.A. McKay, eds.). *Rev. Mineral.* **21**, 309-337.

MARTÍN-IZARD, A., FONTENLA, V., VALÍN, M.L., ARRIBAS, A., MOREIRAS, D., MARCOS-PASCUAL & REGUILÓN, R. (1995): Los ortoneises peralcalinos del borde meridional de la unidad de Malpica – Tuy: caracteres geológicos, mineralógicos, geoquímicos y mineralizaciones de Y–Nb–Zr–TR asociadas. *Estudios Geológicos* **51**, 195-212.

MIYASHIRO, A. (1978): Nature of alkalic volcanic rock series. *Contrib. Mineral. Petrol.* **66**, 91-104.

MONTERO, P. (1993): *Geoquímica y Petrogénesis del Complejo Peralcalino de la Sierra del Galiñeiro (Pontevedra, España).* Ph.D. thesis, Univ. of Oviedo, Oviedo, Spain.

ORTEGA, E. & GIL IBARGUCHI, J.I. (1983): La Unidad de Malpica – Tuy ("Complejo Antiguo" – "Fosa Blastomolinítica"). *In* Geología de España (J.A. Comba, ed.). Libro Jubilar J.M. Rios, Madrid, Spain (430-439).

PIN, C. & MARINI, F. (1993): Early Ordovician continental break-up in Variscan Europe: Nd-Sr isotope and trace element evidence from bimodal igneous associations of the southern Massif Central, France. *Lithos* **29**, 177-196.

________, ORTEGA CUESTA, L.A. & GIL IBARGUCHI, J.I. (1992): Mantle-derived early Paleozoic A-type metagranitoids from the NW Iberian Massif: Nd isotope and trace-element constraints. *Bull. Soc. Géol. France* **163**, 483-494.

Priem, H.N.A., Boelrijk, N.A.I.M., Verschure, R.H., Hebeda, E.H. & Floor, P. (1966): Isotopic evidence for Upper-Cambrian or Lower-Ordovician granite emplacement in the Vigo area, northwestern Spain. *Geol. Mijnbouw* **45**, 36-40.

Prigmore, J.K., Butler, A.J. & Woodcock, N.H. (1997): Rifting during separation of Eastern Avalonia from Gondwana: evidence from subsidence analysis. *Geology* **25**, 203-206.

Pupin, J.-P. & Turco, G. (1972): Une typologie originale du zircon accesoire. *Bull. Soc. fr. Minéral. Cristallogr.* **95**, 348-359.

Rambaud, F., Alvarez, R. & Bonilla, A. (1992): El complejo ígneo peralkalino de Monte Galiñeiro (Vigo – Porriño – Pontevedra), sus mineralizaciones de Y, TRR, Zr, Nb, Th. Investigación preliminar de métodos de concentración. *XV Congr. Mundial de Minería (Madrid*; 789-798).

Ribeiro, M.L. (1987): Petrogenesis of early Paleozoic peralkaline ryolites from the Macedo de Cavaleiros region (NE Portugal). *Geol. Rundsch.* **76**(1), 147-168.

________ & Floor, P. (1988): Magmatismo peralcalino no maciço Hespérico: sua distribuçao e significado geodinamico. *In* Geología de los Granitoides y Rocas Asociadas del Macizo Hespérico (F. Bea, A. Carnicero, J.C. Gonzalo, M. López Plaza & M.D. Rodríguez Alonso, eds.). Ed. Rueda, Madrid, Spain (211-221).

Roeder, P.L. (1985): Electron-microprobe analysis of minerals for rare earth elements: use of calculated peak-overlap corrections. *Can. Mineral.* **23**, 263-271.

Serrano Pinto, M., Casquet, C., Ibarrola, E., Corrtegé, L.G. & Portugal Ferreira, M. (1988): Sintese geocronologica dos granitoides do Maciço Hesperico. *In In* Geología de los Granitoides y Rocas Asociadas del Macizo Hespérico (F. Bea, A. Carnicero, J.C. Gonzalo, M. López Plaza & M.D. Rodríguez Alonso, eds.). Ed. Rueda, Madrid, Spain (69-86).

Taylor, R.P. & Pollard, P.J. (1996): Rare earth element mineralization in peralkaline systems: the T-Zone REE–Y–Be deposit, Thor Lake, Northwest Territories, Canada. *In* Rare Earth Minerals, Chemistry, Origin and Ore Deposits (A.P. Jones, F. Wall & C.T. Williams, eds.). The Mineralogical Society Series **7**. Chapman & Hall, London, U.K. (167-192).

Watson, E.B. (1979): Zircon saturation in felsic liquids: experimental results and applications to trace element geochemistry. *Contrib. Mineral. Petrol.* **70**, 407-419.

________ & Harrison, T.M. (1983): Zircon saturation revisited: temperature and composition effects in a variety of crustal types. *Earth Planet. Sci. Lett.* **64**, 295-304.

Wendlandt, R.F. & Harrison, W.J. (1979): Rare earth partitioning between immiscible carbonate and silicate liquids and CO_2 vapor: results and implications for the formation of light rare earth-enriched rocks. *Contrib. Mineral. Petrol.* **69**, 409-419.

Whalen, J.B., Currie, K.L. & Chappell, B.W. (1987): A-type granites: geochemical characteristics, discrimination and petrogenesis. *Contrib. Mineral. Petrol.* **95**, 407-419.

Wood, S.A. (1990a): The aqueous geochemistry of the rare-earth elements and yttrium. 1. Review of available low-temperature data for inorganic complexes and the inorganic REE speciation of natural waters. *Chem. Geol.* **82**, 159-186.

________ (1990b): The aqueous geochemistry of the rare-earth elements and yttrium. 2. Theoretical predictions of speciation in hydrothermal solutions to 350°C at saturation water vapor pressure. *Chem. Geol.* **88**, 99-125.

Received June 15, 1997, revised manuscript accepted March 15, 1998.